Progress In Electromagnetics Research Letters, Vol. 32, 29–38, 2012

IMPACT OF THE WAVE NUMBER ESTIMATION IN UNDERGROUND FOCUSED SAR IMAGING

F. Quivira*, J. A. Martinez-Lorenzo, and C. M. Rappaport

The Gordon CenSSIS, Northeastern University, 360 Huntington Ave., Suite 302 Stearns Center, MA 02115, USA

Abstract—This work studies the impact of estimating soil wave number in Underground Focused SAR imaging for tunnel detection applications. It is demonstrated that neglecting wave refraction at the ground surface results in poor underground imaging; however, by considering refraction with inexact, yet sufficiently high, estimates of soil dielectric constant, clear target images can be produced. In addition, using a wrong wave number for the soil incorrectly predicts the tunnel's depth, but gives positive identification of its transverse extent.

1. INTRODUCTION

Illicit underground tunnels pose a direct threat to national security, because smugglers use them to traffic explosives, weapons, people, and drugs; furthermore, assailants might use tunnels to burrow below landmarks or high-security facilities in order to detonate dangerous devices. Recently, there have been cases in which illegal tunnels were utilized to avoid the security checkpoints established in the frontier between Mexico and the United States ([1, 2]). In response, several government agencies and research departments throughout the country have investigated several detection methods to prevent illicit tunnels from proliferating. Most of these solutions rely on a Ground Penetrating Radar (GPR) system set up on land ([3–6]). Ground based detection systems are expensive and time consuming because access to terrain above suspected tunnels is often limited or difficult, and examination pace is relatively slow; therefore, there is a high demand for efficient alternatives [7].

Received 5 December 2011, Accepted 23 April 2012, Scheduled 16 May 2012

* Corresponding author: Fernando Quivira (quivira.f@husky.neu.edu).

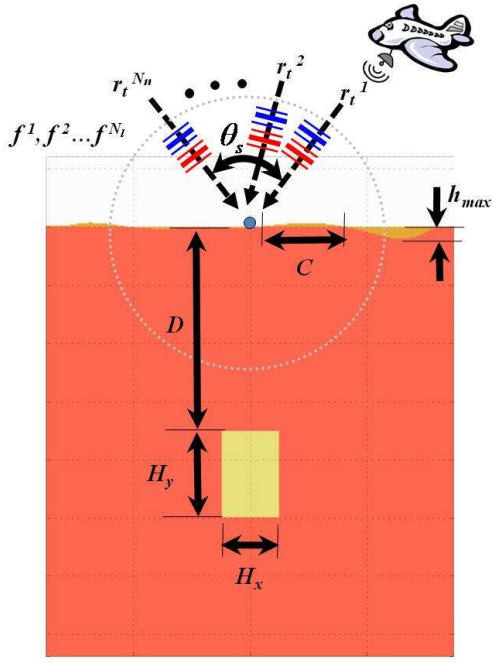

Figure 1. Synthetic aperture radar configuration: Tunnel configuration, schematic of multiple aspect angles, and multiple frequencies per aspect angle.

Synthetic Aperture Radar (SAR) is generally used to create relatively high-resolution images of a known surface region [8, 9]. Synthetic Aperture Radar coupled with Underground Focusing (UF-SAR) has been recently proposed for tunnel detection applications since it is able to sense large areas of terrain in a short amount of time [11, 12]. This sensing method is based on a radar mounted on an aircraft (or multiple radars mounted on multiple planes) that moves over a region of ground with a suspected tunnel. The radar transmits electromagnetic waves at multiple frequencies, which are scattered by the ground and the tunnel. The recorded scattered field is coherently combined for multiple frequencies and positions in order to synthesize an underground spatially localized spot. This underground focusing procedure requires a good approximation of the ground's constitutive parameters. This work studies the impact of uncertainty in the soil's constitutive parameters when performing UF-SAR imaging.

2. UNDERGROUND FOCUSING SYNTHETIC APERTURE RADAR CONFIGURATION

In the UF-SAR algorithm [11, 12], the field $\mathbf{E}\left(f^l,\, \mathbf{r}_t^n,\, \mathbf{r}_r^p\right)$ is measured by the p-th receiving antenna, which is located at $\mathbf{r}_r^p$ (where $p = 1 \ldots N_p$), when the n-th transmitting antenna, which is located at $\mathbf{r}_t^n$ (where $n = 1 \ldots N_n$), is radiating with the l-th frequency f^l (where $l = 1 \ldots N_l$). Thus, the image at the underground point $\mathbf{r}_u^s$ (where $s = 1 \ldots N_s$) is computed as:

$$I\left(\mathbf{r}_u^s\right) = \sum_{l,n,p} \mathbf{E}\left(f^l, \mathbf{r}_t^n, \mathbf{r}_r^p\right) a\left(f^l, \mathbf{r}_t^n, \mathbf{r}_r^p, \mathbf{r}_u^s\right) e^{j\Phi\left(f^l, \mathbf{r}_t^n, \mathbf{r}_r^p, \mathbf{r}_u^s\right)} \tag{1}$$

where $a\left(f^l,\, \mathbf{r}_t^n,\, \mathbf{r}_r^p,\, \mathbf{r}_u^s\right)$ and $\Phi\left(f^l,\, \mathbf{r}_t^n,\, \mathbf{r}_r^p,\, \mathbf{r}_u^s\right)$ are the field amplitude attenuation and phase shift associated with a wave propagating from the transmitting antenna $\mathbf{r}_t^n$ to the receiving antenna $\mathbf{r}_r^p$, when the focusing is performed at $\mathbf{r}_u^s$ (see Fig. 1) [11]. For imaging, the attenuation in the soil, $a\left(f^l,\, \mathbf{r}_t^n,\, \mathbf{r}_r^p,\, \mathbf{r}_u^s\right)$ is assumed to be constant, since the effect of the phase shift component is dominant. In order to compute the phase shift $\Phi\left(f^l,\, \mathbf{r}_t^n,\, \mathbf{r}_r^p,\, \mathbf{r}_u^s\right)$, it is necessary to calculate the refraction point at the air-soil interface. This requires solving a 4th degree polynomial (derived from Snell's Law) that can be approximated by several algorithms [13] or analytical formulation [14]. The path of the propagating wave is shown in Fig. 2. Once the refraction points are derived, the wave vectors (with subscripts 0 and g representing the wave in air and ground respectively):

$$\mathbf{k}_{01} = k_0^l \left(\mathbf{r}_{x1} - \mathbf{r}_t^n\right) / \left|\mathbf{r}_{x1} - \mathbf{r}_t^n\right| \tag{2a}$$

$$\mathbf{k}_{g1} = \Re\left(k_g^l\right) \left(\mathbf{r}_u^s - \mathbf{r}_{x1}\right) / \left|\mathbf{r}_u^s - \mathbf{r}_{x1}\right| \tag{2b}$$

$$\mathbf{k}_{g2} = \Re\left(k_g^l\right) \left(\mathbf{r}_{x2} - \mathbf{r}_u^s\right) / \left|\mathbf{r}_{x2} - \mathbf{r}_u^s\right| \tag{2c}$$

$$\mathbf{k}_{02} = k_0^l \left(\mathbf{r}_r^p - \mathbf{r}_{x2}\right) / \left|\mathbf{r}_r^p - \mathbf{r}_{x2}\right| \tag{2d}$$

can be computed and the phase term in Equation (1) can be written as the sum of the 4 phase terms associated with the wave throughout its traveled path (numbered subscripts are used to denote the 4 stages of the path length from Fig. 2):

$$\begin{aligned} &\Phi_B^{UF}\left(f^l, \mathbf{r}_t^n, \mathbf{r}_r^p, \mathbf{r}_u^s\right) = \phi_1 + \phi_2 + \phi_3 + \phi_4 \\ &\phi_1 = \mathbf{k}_{01} \cdot \left(\mathbf{r}_{x1} - \mathbf{r}_t^n\right), \quad \phi_2 = \mathbf{k}_{g1} \cdot \left(\mathbf{r}_u^s - \mathbf{r}_{x1}\right) \\ &\phi_3 = \mathbf{k}_{g2} \cdot \left(\mathbf{r}_{x2} - \mathbf{r}_u^s\right), \quad \phi_4 = \mathbf{k}_{02} \cdot \left(\mathbf{r}_r^p - \mathbf{r}_{x2}\right) \end{aligned} \tag{3}$$

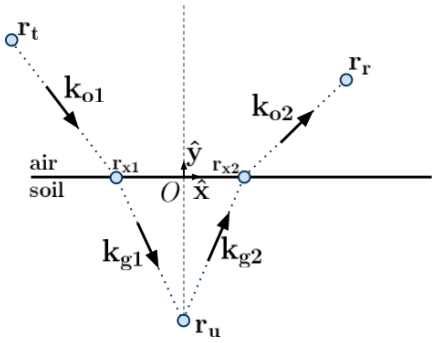

Figure 2. Modeled path of the wave propagating from the transmitting antenna at $\mathbf{r}_t$ to the receiving antenna at $\mathbf{r}_r$ when the underground focusing is performed at $\mathbf{r}_u$.

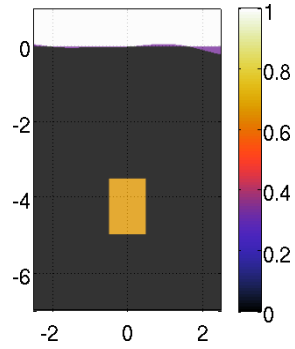

Figure 3. Soil half space with geometry shown in Fig. 3. This scenario was used as problem geometry in the finite difference in frequency domain (FDFD) analysis. Axes are shown in meters. Yellow represents a tunnel surrounded by rough soil.

The wave numbers in air $k_0^l = 2\pi f^l \sqrt{\mu_0 \epsilon_0}$ and in the soil $k_g^l = 2\pi f^l \sqrt{\mu_0 \epsilon' \epsilon_0}$ (where μ_0 and ϵ_0 is the permittivity and permeability on the air, and ϵ' is the relative complex permittivity of the ground) are required to perform the imaging. The main problem encountered when performing the latter procedure is that the complex permittivity on the ground is generally unknown, and a guess of such quantity is needed to reconstruct an image of the subsurface.

Throughout this paper, only the special case of Multiple Monostatic (MM) configuration will be considered, i.e., the transmitting and receiving antennas are mounted on the same moving aircraft. Therefore, $\mathbf{r}_t^n = \mathbf{r}_r^n$ and Equation (1) can be written as:

$$I\left(\mathbf{r}_u^s\right) = \sum_{l,n} \mathbf{E}\left(f^l, \mathbf{r}^n\right) e^{j\Phi\left(f^l, \mathbf{r}^n, \mathbf{r}_u^s\right)} \tag{4}$$

In addition, the phase term, given by Equation (3), can be simplified since ϕ_1 is equal to ϕ_4 and ϕ_2 is equal to ϕ_3. As a result, the associated phase shift is proportional to twice the electrical distance existing between the antenna position and the focusing point, and it can be written as:

$$\Phi_2\left(f^l, \mathbf{r}_t^n, \mathbf{r}_r^p, \mathbf{r}_u^s\right) = 2\left(\phi_1 + \phi_2\right) \tag{5}$$

3. NUMERICAL RESULTS: IMPACT OF FOCUSING WITH DIFFERENT WAVE NUMBERS

A Finite Difference Frequency Domain (FDFD) analysis algorithm developed by [15–17] is used to numerically generate scattered fields from a soil half-space with a rough ground surface. Note that the FDFD model implicitly solves a system of simultaneous equations in terms of the spatially discretized field values for each fixed single frequency at a time, much like the finite element method. It is not a time domain method, like FDTD, and as such correctly computes the frequency-dependent wave attenuation and velocity through the lossy soil. In addition, the numerical simulation has been validated in [19].

The tunnel detection simulation was performed on two soil scenarios: non-dispersive dry clay and lossy moist clayey loam. The dry clay ground was characterized by a permittivity of $\epsilon = \epsilon_0(8-j0.01)$. Although this is unusually high for most dry soils, it provides a challenging scattering geometry for reconstruction [18]. Similar tests and results have been found for the easier case of dry sand with $\epsilon = \epsilon_0(2.55 - j0.01)$ [11, 18]. The lossy loam ground was characterized as A. P. Hill Firing Point 20 soil with permittivity and conductivity shown in Fig. 4. In addition, the general parameters of the problem are listed in Table 1 [11].

3.1. Non-dispersive Dry Clay

For the image reconstruction, the estimated soil permittivity was tested parametrically, varying from $\hat{\epsilon}' = 1$ to $\hat{\epsilon}' = 12$. Fig. 5 presents the UF-

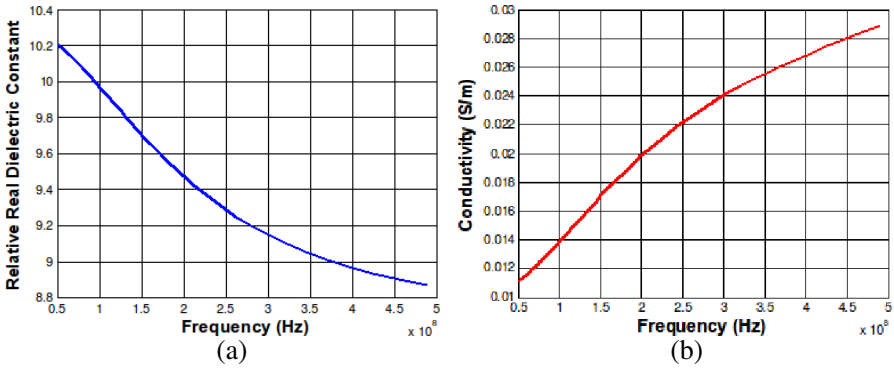

Figure 4. A. P. Hill firing point 20 soil dielectric characteristics as a function of frequency.

Table 1. Parameters for the baseline configuration.

TUNNEL	
Tunnel height	$H_y = 1.5\,\mathrm{m}$
Tunnel width	$H_x = 1\,\mathrm{m}$
Tunnel depth	$D = 3.5\,\mathrm{m}$
ROUGH SURFACE	
Correlation factor	$C = 1\,\mathrm{m}$
Amplitude height	$h_{\max} = .1\,\mathrm{m}$
RADAR SOURCE	
Center frequency	$f_c = 300\,\mathrm{MHz}$
Bandwidth	$BW = 500\,\mathrm{MHz}$
Range resolution in air	$\Delta R = 0.6\,\mathrm{m}$
Number of frequencies	$N_l = 128$
TRANSMISSION (equally angle-spaced plane waves)	
Number of transmitting antennas	$N_a = N_n = 19$
Center angle	$\theta_c = 0°$
Subtended angle	$\theta_s = 90°$
Cross range resolution in air	$\Delta R_x \approx .64\,\mathrm{m}$
RECEPTION FAR (equally angle-spaced point sources)	
Number of receiving antennas	$N_p = 19$
Position in m of the first element	$\mathbf{r}_r^1 = -100\hat{\mathbf{x}} + 100\hat{\mathbf{y}}$
Position in m of the last element	$\mathbf{r}_r^{19} = 100\hat{\mathbf{x}} + 100\hat{\mathbf{y}}$

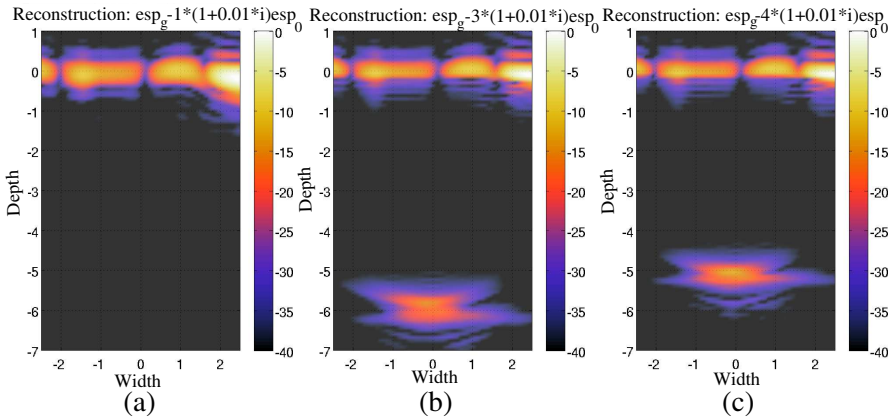

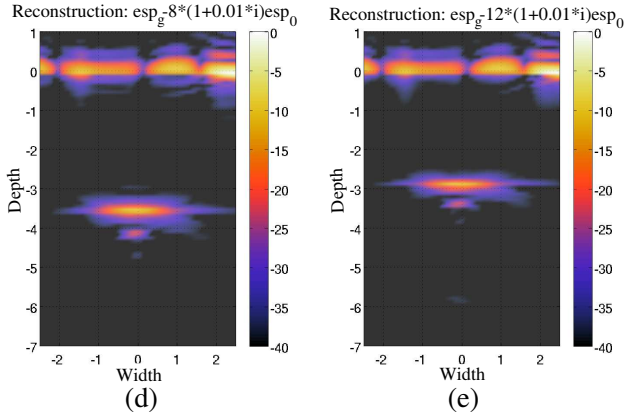

Figure 5. UF-SAR images for a sandy soil half space with geometry shown in Fig. 3. The imaging algorithm assumes a real relative permittivity of, (a) $\epsilon' = 1$, (b) $\epsilon' = 3$, (c) $\epsilon' = 4$, (d) $\epsilon' = 8$, (e) $\epsilon' = 12$. The images are in dB scale.

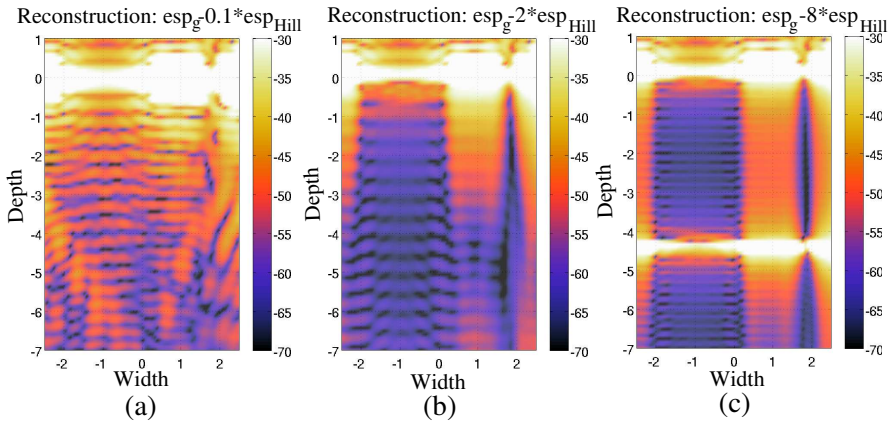

Figure 6. UF-SAR images for a lossy clay soil half space with geometry shown in Fig. 3, but with a rough ground surface of 0.01 [m] average height variation. The imaging algorithm assumes a dielectric constant of: (a) $\hat{\epsilon} = 0.1\epsilon_{\text{A. P. Hill}}$, (b) $\hat{\epsilon} = 2\epsilon_{\text{A. P. Hill}}$, (c) $\hat{\epsilon} = 8\epsilon_{\text{A. P. Hill}}$. The images are in dB scale.

SAR images obtained for five different representative cases. The top of the tunnel can be easily distinguished for each case with $\hat{\epsilon}' \geq 4$. The primary imaging error from using the wrong wave number is that the predicted depth of the tunnel is incorrect. If the estimated permittivity

used in the imaging is too small relative to the true permittivity, the tunnel image is poor (Fig. 5). However, even for the 50% underestimate of $\hat{\epsilon}' = 4$, the tunnel response is clear.

3.2. Lossy Clayey Loam

In this particular scenario, the estimated soil dielectric constant used in the imaging algorithm varied from $\hat{\epsilon} = 0.1\epsilon_{\text{A. P. Hill}}$ to $\hat{\epsilon} = 8\epsilon_{\text{A. P. Hill}}$. Fig. 6 shows how the tunnel response is obscured by the surface clutter. The target signal attenuates rapidly due to the constitutive parameters of this particular soil. In these three representative cases (shown in Fig. 6), imaging with a wrong wave number was not enough to detect the presence of an underground tunnel, even for the unrealistically small value of surface roughness.

4. CONCLUSIONS

This work has addressed the impact of using different wave number estimates for soil in determining the refraction focusing to produce UF-SAR images. It has been shown that using a sufficiently high but incorrect wave number on low loss soils can accurately predict the transverse tunnel position, but fails to correctly reconstruct the tunnel's depth. In particular, tunnels buried in non-dispersive dry soil were detectable. On lossy clay soils, the surface clutter overshadowed the dim tunnel signal. This study demonstrates that as long as the soil is not too lossy, such as in desert regions, tunnels can be successfully detected using refraction focusing without precisely knowing the actual wave number. Further experimental work is on-going, and will be reported in a subsequent paper.

ACKNOWLEDGMENT

This work is supported by CenSSIS, the Gordon Center for Subsurface Sensing and Imaging Systems NSF ERC Program (Award number EEC-9986821). In addition, this material is based upon work supported by the U.S. Department of Homeland Security under Award Number 2008-ST-061-ED0001. The views and conclusions contained in this document are those of the authors and should not be interpreted as necessarily representing the official policies, either expressed or implied, of the U.S. Department of Homeland Security.

REFERENCES

1. U.S. Customs and Border Protection Agency, "Agents investigate new tunnel found in nogales," December 2009, [Online]. Available: http://www.cbp.gov/xp/cgov/newsroom/news_releases/archives/2009_news_releases/dec_2009/12302009_3.xml.
2. U.S. Customs and Border Protection Agency, "U.S. border patrol agents foil two smuggling attempts," May 2009, [Online]. Available: http://www.cbp.gov/xp/cgov/newsroom/news_releases/archives/2009_news_releases/may_2009/05112009_2.xml.
3. Lo Monte, L., D. Erricolo, F. Soldovieri, and M. Wicks, "Radio frequency tomography for tunnel detection," *IEEE Transactions on Geoscience and Remote Sensing*, Vol. 48, No. 3, 1128–1137, 2010.
4. West, P., "Tunnel and subsurface void detection and range to target measurement," *IEEE Conference on Technologies for Homeland Security*, 677–684, 2009,.
5. Carin, L., J. Sichina, and J. Harvey, "Microwave underground propagation and detection," *IEEE Transactions on Microwave Theory and Techniques*, Vol. 50, No. 3, 945–952, 2010.
6. Brown, R., E. Lynch, D. Mokry, J. VanDamme, R. Schneible, and M. Wicks, "Near field focusing algorithm for high frequency ground penetration imaging radar," *The Record of the 1999 IEEE Radar Conference*, 66–71, 1999.
7. Department of Homeland Security, "Tunnel detection technologies project," January 2007, [Online]. Available: https://baa.st.dhs.gov/Solicitations/BAA07-01A_TunnelDetectionTechnologiesProject.pdf.
8. Skolnik, M., *Radar Handbook*, McGraw-Hill, USA, 2008.
9. Carrara, W. G., R. S. Goodman, and R. M. Majewski, *Spotlight Synthetic Aperture Radar: Signal Processing Algorithms*, Artech House, Inc., USA, 1995.
10. Chan, Y. K., B.-K. Chung, and H.-T. Chuah, "Transmitter and receiver design of an experimental airborne synthetic aperture radar sensor," *Progress In Electromagnetics Research*, Vol. 49, 203–218, 2004.
11. Martinez, J., C. Rappaport, and F. Quivira, "Physical limitations on detecting tunnels using underground focusing synthetic aperture radar," *IEEE Transactions on Geoscience and Remote Sensing*, Vol. 49, No. 1, 65–70, 2011.
12. Martinez-Lorenzo, J. and C. Rappaport, "Underground focusing spotlight synthetic aperture radar for tunnel detection applica-

tions," *IEEE International Symposium on Antennas and Propagation*, 1–4, 2009.

13. Johansson, E. M. and J. E. Mast, "Three-dimensional ground penetrating radar imaging using synthetic aperture time-domain focusing," *Conference on Advanced Microwave and Milimeter Wave Detectors*, 205–214, 1994.
14. Rappaport, C., "Accurate determination of underground GPR wavefront and B-scan shape from above-ground point sources," *IEEE Transactions on Geoscience and Remote Sensing*, Vol. 45, No. 8, 2429–2434, 2007.
15. Rappaport, C. and A. Morgenthaler, "FDFD modeling of plane wave interactions with buried objects under rough surfaces," *IEEE International Symposium on Antennas and Propagation*, 318, 2001.
16. Marengo, E., C. Rappaport, and E. Miller, "Optimum PML ABC conductivity profile in FDFD," *IEEE Transactions on Magnetics*, Vol. 35, No. 3, 1506–1509, 1999.
17. Rappaport, C., M. Kilmer, and E. Miller, "Accuracy considerations in using the PML ABC with FDFD Helmholtz equation computation, *IEEE Transactions on Magnetics*, Vol. 13, No. 471, 471–482, 2000.
18. Von Hippel, A. R., *Table of Dielectric Materials*, MIT Press, USA, 1953.
19. Farid, A., J. Martinez-Lorenzo, A. Alshanabkeh, and C. Rappaport, "Experimental validation of a numerical forward model for tunnel detection using cross-borehole radar," *ASCE, Journal of Geotechnical and Geoenvironmental Engineering*, 2012.